Spatial Coherence Manipulation on the Statistical Photonic Platform

Leixin Liu
Soochow University
Wenwei Liu
Nankai University
Fei Wang
Soochow University
Hua Cheng
Nankai University
Duk-Yong Choi
The Australian National University https://orcid.org/0000-0002-5339-3085
Jianguo Tian
Nankai University
Yangjian Cai
Soochow University
Shuqi Chen (schen@nankai.edu.cn)
Nankai University

Article

Keywords: spatial coherence, coherence manipulation, light fields, statistical photonic platform

Posted Date: September 23rd, 2021

DOI: https://doi.org/10.21203/rs.3.rs-888780/v1

Spatial Coherence Manipulation on the Statistical Photonic Platform

Leixin Liu[1], Wenwei Liu[2,*], Fei Wang[1], Hua Cheng[2,*], Duk-Yong Choi[4], Jianguo Tian[2], Yangjian Cai[1,3,*], and Shuqi Chen[2,5,6,*]

[1]School of Physical Science and Technology, Soochow University, Suzhou 215006, China

[2]The Key Laboratory of Weak Light Nonlinear Photonics, Ministry of Education, Renewable Energy Conversion and Storage Center, School of Physics and TEDA Institute of Applied Physics, Nankai University, Tianjin 300071, China

[3]Shandong Provincial Engineering and Technical Center of Light Manipulation & Shandong Provincial Key Laboratory of Optics and Photonic Device, School of Physics and Electronics, Shandong Normal University, Jinan 250014, China

[4]Laser Physics Centre, Research School of Physics, Australian National University, Canberra, ACT 2601, Australia

[5]The Collaborative Innovation Center of Extreme Optics, Shanxi University, Taiyuan, Shanxi 030006, China.

[6]The Collaborative Innovation Center of Light Manipulations and Applications, Shandong Normal University, Jinan 250358, China

**Corresponding author, email: wliu@nankai.edu.cn; hcheng@nankai.edu.cn; yangjiancai@suda.edu.cn; schen@nankai.edu.cn*

Abstract:

Coherence, like amplitude, polarization and phase, is a fundamental characteristic of the light fields and is dominated by the statistical optical property. Generally, accurate coherence manipulation is challenging since coherence as a statistical quantity requires the combination of various bulky optical components and fast tuning of optical media. Spatial coherence as another pivotal optical dimension still has not been significantly manipulated on the photonic platform. Here, we theoretically and

experimentally realize accurate manipulation of the spatial coherence of light fields by loading a temporal random phase distribution onto the wave-front on the statistical photonic platform. By quantitatively manipulating the statistical photonic properties, we can successfully achieve the partially coherent light with the pre-defined degree of coherence and continuously modulate it from fully coherent to incoherent. This design strategy can also be easily extended to manipulate the spatial coherence of other special beams such as partially coherent vortex beam generations. Our approach provides straightforward rules to manipulate the coherence of the light fields and paves the way for applications of partially coherent beams in information encryption, ghost imaging, and information transmission in turbulent media.

Introduction

Coherence is one of the most important concepts in optics and is strongly related to the ability of light to exhibit interference effects. The statistical optical property as a fundamental characteristic dominates the coherence of electromagnetic waves (EMWs)[1,2], which has boosted the development of lasers, precision measurements, and information transmission. The beams with partial coherence have been applied in various fields, such as plasma-instability suppression[3], varying polarization modes[4], structuring random solitons[5], ghost imaging[5-7] and optical communication, which can significantly reduce the scintillation and beam wandering caused by turbulent atmosphere[8]. However, the generation of partially coherent beams traditionally requires a combination of various optical components such as lenses, rotating ground glass, and a spatial light modulator with specific distances in between[9,10], which is complex, bulky, and is challenging to be integrated on a single photonic platform. The degree of coherence (DOC) is also challenging to be accurately manipulated due to the inevitable statistical roughness of the ground glass or other disordered media.

In the past decade, metasurfaces have attracted much attention due to their great potentials in integrated optical systems and advanced photonics. By tailoring the geometric parameters and spatial symmetry of the sub-wavelength metallic or dielectric building blocks, versatile local resonances such as waveguide modes[11], Fano resonances[12,13], and bound states in the continuum[14-16] can be generated, which strikingly boosts the light-matter interactions between EMWs and the nano-structures. Such resonances locally introduce abrupt changes in optical components in an ultra-

thin plane, leading to significant wave-front[17-19] and polarization[20-22] manipulation of EMWs. Although several optical dimensional manipulations have been systematically investigated, such as amplitude, polarization, and phase of EMWs[23-27], which have been applied in sub-resolution focusing[28], arbitrary spin-to-orbital angular momentum conversion[29], and information photonics[26], the spatial coherence as another pivotal optical dimension has not been significantly manipulated, especially in the photonic platform. Generally, coherence manipulation is challenging since coherence as a statistical quantity requires either fast tuning of optical media or fabricating numerous different samples. Recently, researchers engineered the individual input-output responses with disordered metasurfaces to realize the wavefront shaping[30]. However, the wide range of statistical optical properties and their applications on the photonic platform still have not been revealed and quantitatively studied.

Here, we introduce a strategy with statistical metasurfaces to accurately manipulate the spatial coherence of EMWs by projecting a temporal random phase distribution onto the wave-front. The statistical photonic properties such as information entropy are quantitatively demonstrated and the partially coherent vortex beams with the pre-defined DOC can be successfully obtained on the statistical photonic platform. The experimental results meet well with the theoretical predictions. The proposed strategy can also be easily extended to manipulate the spatial coherence of other special beams such as partially coherent vortex beam generations. Our approach paves the way for a new direction in statistical photonic manipulation and provides a routine to apply partially coherent beams in the information photonic

systems.

Results

Concept of the statistical metasurfaces. To quantify the statistical properties on the photonic platform, we start from the harmonic formula of the electric fields of EMWs:

$$E(\mathbf{r},t) = A(\mathbf{r})\exp\left[i\varphi(\mathbf{r},t)\right], \tag{1}$$

where $A(\mathbf{r})$ and $\varphi(\mathbf{r}, t)$ denote the amplitude and phase of the electric fields at an arbitrary point $\mathbf{r}$, respectively. Generally, the statistical behavior of $\varphi(\mathbf{r}, t)$ decides the coherence of the EMWs, which can be described by the mutual coherence function (MCF) in the space-time domain[31]:

$$\Gamma(\mathbf{r}_1,\mathbf{r}_2,\tau) = \left\langle E(\mathbf{r}_1,t_1)E^*(\mathbf{r}_2,t_2)\right\rangle, \tag{2}$$

where $\tau = t_2 - t_1$, the asterisk denotes the complex conjugate and the angle brackets denote an ensemble average over the fluctuating field. By substituting Eq. (1) to Eq. (2), the MCF can be express as:

$$\Gamma(\mathbf{r}_1,\mathbf{r}_2,\tau) = A(\mathbf{r}_1)A^*(\mathbf{r}_2)\left\langle \exp\left[i\varphi(\mathbf{r}_1,t_1) - i\varphi^*(\mathbf{r}_2,t_2)\right]\right\rangle, \tag{3}$$

where we assume $A(\mathbf{r})$ does not change with $\mathbf{r}$ for convenience both in theory and experiments. Specifically, for narrowband or quasi-monochromatic EMWs the longitudinal coherent length of the light is much greater than the maximum path-length difference between $\mathbf{r}_1$ and $\mathbf{r}_2$ to the observation point. Thus, the MCF is a slow varying function in the τ domain, and can be simplified to a mutual intensity function $\Gamma(\mathbf{r}_1, \mathbf{r}_2) = \Gamma(\mathbf{r}_1, \mathbf{r}_2, \tau = 0)$. Accordingly, the degree of the spatial coherence of a scalar partially coherent beam takes the form:

$$\mu(\mathbf{r}_1,\mathbf{r}_2) = \frac{\Gamma(\mathbf{r}_1,\mathbf{r}_2,\tau=0)}{\sqrt{\Gamma(\mathbf{r}_1,\mathbf{r}_1)\Gamma(\mathbf{r}_2,\mathbf{r}_2)}}. \tag{4}$$

By substituting Eq. (3) to Eq. (4), we obtain the correlation of the EMWs at two arbitrary points:

$$\mu(\mathbf{r}_1,\mathbf{r}_2)=\left\langle \exp\left[i\varphi(\mathbf{r}_1,t_1)-i\varphi^*(\mathbf{r}_2,t_2)\right]\right\rangle. \tag{5}$$

Obviously, the coherence of a beam is essentially phase-dependent, which means we can change the coherence of a beam by imposing different local phase fluctuations upon the EMWs. The phase fluctuation of $\varphi(\mathbf{r}, t)$ can be arbitrarily designed, leading to a wide range of partially coherent beams with various kinds of coherence functions that can be applied in different scenarios, such as overcoming the Rayleigh diffraction limit in optical imaging systems[32] and optical trapping[33]. Recent developments in photonics and metasurfaces, which provide versatile capabilities to manipulate different optical dimensions, have enabled accurate engineering of the wave-front of EMWs pixel by pixel[27,34]. Taking advantage of the high-efficiency manipulation of transmitted Pancharatnam-Berry (P-B) phase in titanium dioxide nanofins, we propose a strategy to accurately manipulate partially coherent beams with a pre-defined DOC. The schematic of the coherence-manipulated design is shown in Fig. 1(a). Here, each unit cell S_i of the sample is regarded as a phase pinhole, and the coherence properties of the phased array are decided by the interferences of every two pinholes, which can be measured through Young's double-slit interference experiment [Fig. 1(b)][35]. The statistical fluctuations of the transmitted fields arise from the randomly arranged nanostructures of the phased array. Theoretically, the instantaneous light intensity of the beam generated by the statistical metasurface is Gaussian-enveloped with speckles as shown in Fig.1(c), and the size of speckle <d> is

related to the coherence of the transmitted beam. By controlling the scanning of the statistical metasurface along the *x*-direction, the wave-front of the output EMWs is spatially modulated, which statistically results in a specific DOC of the beam.

Implementation of the statistical metasurfaces with uniformly disordered phase fluctuation. A proof-of-concept design to demonstrate the proposed strategy is shown in Fig. 2. To obtain the statistical properties of the metasurfaces, we bring in a disorder-manipulated phase distribution and employ six regions of the statistical metasurface to generate six partially coherent beams with different spatial coherence (Fig. 2a,b). The phase of the statistical metasurface in Region #*i* randomly and uniformly covers the phase fluctuation range (PFR) of $[\pi-0.2\times(i-1)\pi, \pi+0.2\times(i-1)\pi]$, and in each region an ensemble statistical analysis is performed. Specifically, in Region #1 the statistical metasurface serves as a uniform phase-distributed plate without phase difference modulation, and the transmitted beam is a perfect Gaussian beam without intensity speckles, which means the output light is fully coherent. While in Region #6 the statistical metasurface has completely phase-disordered from 0 to 2π, resulting in nearly incoherent transmitted light. Note that the uniformly distributed phase design in Fig. 2a is not unique, and the different random distributed functions can lead to different coherence structures with the proposed strategy in Fig. 2b. The building blocks of the statistical metasurfaces are TiO_2 nanofins with a length of 260 nm, a width of 90 nm, and a height of 550 nm. The lattice size of the statistical metasurface is 330 nm. The transmitted phase can be locally manipulated following the P-B phase formula $\varphi(\mathbf{r}) = 2\sigma\theta(\mathbf{r})$, where $\sigma = \pm 1$ represents the left-/right-handed

circularly polarized incident light, and θ is the local orientation angle of the nanofin (Fig. 2c). Such large aspect-ratio dielectric structures with high refractive index can generate waveguide modes and support Fabry-Pérot resonances, realizing the transmitted phase modulation with a high efficiency of more than 93%, which is challenging in traditional platforms such as the ground glasses or the spatial light modulator. Figure 2d shows the calculated information entropy with increasing of the disorder of the phase distribution. The information entropy is calculated through:

$$H(\varphi) = -\sum_{j=1}^{N} \frac{1}{p_j(\varphi)} \log_N \left(p_j(\varphi) \right), \tag{6}$$

where N is the number to evenly segment the phase interval 0–2π, $p_j(\varphi)$ is the possibility of the phase located in the j-th interval. Compared with conventional information entropy using 2 as the base of the logarithm[36], here we employ N as the base to obtain convergent results, which changes the unit system in definition (see Supplementary Fig. 1 for different value of N and the comparison with taking 2 as the base). The disordered phases result in different sizes of speckles of the instantaneous intensity of the transmitted light (insets in Fig. 2d). The statistical metasurface can be readily fabricated with the standard atomic layer deposition method[37,38] through single-step lithography. The scanning electron micrograph of the fabricated sample in our experiments is shown in Fig. 2e. The total size of the fabricated statistical metasurface is 240 μm, and the size of each region is 240 μm × 40 μm. More details about the sample fabrication can be found in Method.

A left-handed circularly polarized Gaussian beam with beam size of 30 μm is focused onto the statistical metasurface, which is a bit smaller than each region of the

statistical metasurface to avoid information crosstalk. An electric translation stage controls the movement of the statistical metasurface along the *x*-direction, loading a temporal phase change to the wave-front within a limited phase coverage. The transmitted cross-polarized light was captured by an imaging system to record the light distributions. We obtained six groups of the instantaneous intensity distributions captured by the CCD camera while scanning the statistical metasurface. The measured instantaneous intensities of different phase fluctuation setups show significant intensity speckle in Fig. 3a-e, which is one of the evidences of the partially coherent beams. The defects in the light distribution can be attributed to fabrication imperfections. The average intensities in Fig. 3a-e are the statistical average of the square of modulus of fluctuating EMWs at point $\mathbf{r}$, i.e., $\mathbf{r} = \mathbf{r}_1 = \mathbf{r}_2$ in Eq. (2), which are calculated by averaging the $\times 1000$ instantaneous intensity distributions. A video recording of the measured instantaneous intensity distributions for different PFRs while scanning is shown in Supplementary Video 1. When the scanning speed of the beam on the platform is fast enough, a real-time averaged intensity distribution of the generated beam is feasible in experiment. The beam width w_0 of the generated speckled beams can be analyzed by adopting a theoretical Gaussian curve-fitting of the average intensity distributions. Figure 3f shows the fluctuation of the measured full width at half maximum (FWHM) of the speckles for different PFRs, which apparently fluctuates in a limited range and decreases as the PFR increases. Such fluctuation statistically determines the coherent properties of the transmitted beam. The speckle can be viewed as a coherent superposition of the incident light, and the

light coming from the speckle should also be coherent[39]. In contrast, the light coming from different light speckles is separated by different superposition processes, such as the low-intensity areas between the speckles resulting from statistically averaged superposition. Thus, the size of the speckles can sever as a significant indicator of the coherence of the beam. The smaller the speckle is, the lower the spatial coherence will be. Figure 3g illustrates the detailed experimental setup for capturing the aforementioned instantaneous intensity distributions in Fig. 3a-e.

Spatial coherence manipulation of the statistical metasurfaces. The output light distributions captured by the CCD camera can be statistically analyzed to measure the normalized fourth-order correlation function (FOCF)[40], which is defined as:

$$g^{(2)}\left(\mathbf{r}_1,\mathbf{r}_2\right)=\frac{\left\langle I\left(\mathbf{r}_1,t\right)I\left(\mathbf{r}_2,t\right)\right\rangle}{\left\langle I\left(\mathbf{r}_1,t\right)\right\rangle\left\langle I\left(\mathbf{r}_2,t\right)\right\rangle}, \tag{7}$$

where the angle brackets denote the time average and I ($\mathbf{r}$, t) is the instantaneous intensity distribution. Since the probability distribution of the random phase embedded in the sample is spatially uniform, the random process is ergodic while scanning the sample. Thus, one can use the time average over the correlation of the sequence of instantaneous intensity distributions between $\mathbf{r}_1$ and $\mathbf{r}_2$ to measure the spatial coherence width of the fields, instead of employing an ensemble average. Particularly, the normalized FOCF is linearly dependent on the square of the modulus of DOC function provided that the random process obeys the Gaussian statistics, i.e.,

$$g^{(2)}\left(\mathbf{r}_1,\mathbf{r}_2\right)=1+\left|\mu\left(\mathbf{r}_1,\mathbf{r}_2\right)\right|^2. \tag{8}$$

In the experiment, a series of pictures were captured by a CCD camera during the scanning process, and each picture shows one instantaneous intensity distribution of

the beam cross-section. Each instantaneous intensity can be characterized by a matrix, $I^{(m)}(x, y)$, where x and y are in pixel coordinates, and m denotes the index of each instantaneous intensity. The FOCF can be expressed as the discrete form:

$$g^{(2)}(\mathbf{r}_1, \mathbf{r}_2) = \frac{\frac{1}{M}\sum_{m=1}^{M} I^{(m)}(\mathbf{r}_1) I^{(m)}(\mathbf{r}_2)}{\bar{I}(\mathbf{r}_1)\bar{I}(\mathbf{r}_2)}, \tag{9}$$

where $\bar{I}(\mathbf{r}_1)$ and $\bar{I}(\mathbf{r}_2)$ denote the average intensity at point $\mathbf{r}_1$ and $\mathbf{r}_2$, respectively, which are given by:

$$\bar{I}(\mathbf{r}_i) = \sum_{m=1}^{M} I^{(m)}(\mathbf{r}_i)/M, \quad (i=1,2). \tag{10}$$

The recorded pictures were post-processed through MATLAB to calculate the FOCF using Eq. (9). We took M = 1000 pictures of the instantaneous intensity to achieve convergent results of FOCF, which can determine the spatial coherence width of the output beam.

Figure 4 further demonstrates the spatial coherence manipulation based on the statistical metasurfaces. The intensity distribution of the fully coherent Gaussian beam through Region #1 is given in Fig. 4a. Figure 4b shows experimental results of $|\mu(\mathbf{r}_1, \mathbf{r}_2 = 0)|^2$, i.e., the square of the modulus of the DOC, of the modulated partially coherent beams for different PFRs. The square of the modulus of the DOC of the modulated beams is Gaussian-enveloped according to the Gaussian Shell Model[41]. The theoretical Gaussian curve-fittings were adopted to obtain the coherent length of the beams, as shown in Fig. 4b. Although the Gaussian curve-fitting varies for different cut-line orientation angles (defined as the intersection with the +y direction), the calculated DOC only suffers from limited fluctuations for a specific PFR (Fig. 4c

and the inset). The Gaussian curve-fittings for different θ and PFRs can be found in Supplementary Fig. 2. We also calculated the global coherence $\eta = \delta_0 / w_0$ for each PFR, where δ_0 denotes the coherent length of the output beam obtained via the theoretical fit, and w_0 denotes the beamwidth of the output beam in the experiments. Figure 4d shows the comparison between the theoretical and measured global coherence η of the output light for different PFRs, demonstrating that the proposed scheme can efficiently manipulate the global coherence of light from full coherence to incoherence.

Spatial coherence manipulation of other special beams. Our proposed method can conveniently manipulate the spatial coherence of different special beams in a wide range. Generally, the special beam can be realized through a transmission screen $T(x, y)$ with specific amplitude and phase distributions. The complex envelope of the transmitted light is described as:

$$A_t(x, y, t) = A_i(x, y, t - \tau_0) T(x, y), \tag{11}$$

where A_i is the complex envelope of the incident light, τ_0 is the average time delay associated with the metasurface. Thus, the mutual intensity of the transmitted light is:

$$\begin{aligned} \Gamma_t(x_1, y_1; x_2, y_2) &= \left\langle A_t(x_1, y_1, t) A_t^*(x_2, y_2, t) \right\rangle \\ &= T(x_1, y_1) T^*(x_2, y_2) \left\langle A_t(x_1, y_1, t - \tau_0) A_t^*(x_2, y_2, t - \tau_0) \right\rangle. \end{aligned} \tag{12}$$

Accordingly, the general relationship between the incident and transmitted mutual intensity is:

$$\Gamma_t(x_1, y_1; x_2, y_2) = T(x_1, y_1) T^*(x_2, y_2) \Gamma_i(x_1, y_1; x_2, y_2), \tag{13}$$

where $\Gamma_i(x_1, y_1; x_2, y_2)$ is the mutual intensity of the incident light. Specifically, when $T(x, y)$ is a unitary phase mask, the DOC of the transmitted beam is the same as that

of the incident beam. Thus, we can load a unitary phase mask onto the generated partially coherent beam, and obtain a special beam with the same spatial coherence. To demonstrate the spatial coherence manipulation of the special beams, we employed a vortex phase plate on the transmission path of the generated partially coherent beam (Fig. 5). The calculated intensity distributions of the partially coherent vortex beams with different coherences are shown in Fig. 5a and the corresponding measured results captured by the CCD camera are shown in Fig. 5b. The vortex phase plate adds an additional wavefront to the partially coherent beam generated by the statistical metasurface, which will not alter the beam width and spatial coherence. The central dark spot of the doughnut intensity profile for the partially coherent vortex beam phenomenologically becomes smaller and weaker with decreasing of the spatial coherence resulting from increasing of the disorder of the random phase distribution. Similar operations can also be applied in phase-only partially coherent hologram generation.

Discussion

Traditionally the DOC of the beam has to be measured before further applications, while in our strategy the DOC of the generated beam can be predefined and accurately manipulated. It is noteworthy that the limitation of phase-only-based partially coherent special beam generation is not fundamental, the transmission screen $T(x, y)$ with arbitrary amplitude and phase distribution can also be applied. The difference is that the coherence distribution will change when loading the mask $T(x, y)$, but the DOC of such special beams still can be determined through Eq. (13). The proposed

statistical scheme simplifies the experimental setups for the spatial coherence manipulation of light, and provides the possibilities for further statistically characteristics and applications on an ultracompact photonic platform. Compared with traditional methods to control the spatial coherence of light by employing bulky disordered media, our approach also significantly reduces the energy loss of the incident light, which further promotes the applications of partially coherent beams. Although we employ a mechanical method to modulate the random phase distributions at the seconds level, the tuning speed limitation is not fundamental. For example, the spatial coherence manipulation can be real-time modulation by adopting a micro-electromechanical system[42] or employing structured light[43] to scan the sample.

In summary, we propose a design strategy to accurately manipulate the spatial coherence of EMWs by loading a temporal random phase distribution onto the wave-front on the statistical photonic platform. The proposed statistical metasurface consists of high-efficiency dielectric nanofins that can locally manipulate the correlation between different locations of EMWs, leading to partially coherent light with a pre-defined DOC. We demonstrate for the first time that the output beam can be continuously modulated from fully coherent to incoherent on the statistical photonic platform. We also demonstrate the statistical properties of the metasurface such as information entropy and apply this design strategy to partially coherent vortex beams generations, and the experimental results meet well with the theoretical predictions. This strategy not only significantly simplifies the experimental setups to realize partially coherent beams, but also enables pre-designed and accurate

manipulation of the spatial coherence for different kinds of light beams. Our approach paves the way to generate partially coherent beams with extraordinary correlation functions on the statistical photonic platforms, which can boost the applications in information photonics such as turbulent information transmission and information retrieval in disordered or perturbative media.

Methods

Sample fabrication. The dielectric statistical TiO_2 metasurfaces were fabricated on a cleaned fused silica substrate. Firstly, a layer of 550 nm electron-beam resist (ZEP 520A from Zeon) was spin-coated on the substrate, then baked on a hot plate at 180 °C for 1 min. To prevent charging during electron-beam writing, a thin layer of the E-spacer 300Z (Showa Denko) was coated on the resist. The nanostructures were defined by electron-beam lithography (Raith150) at 30 kV with 20-pA current and 80 $\mu C/cm^2$ dose, followed by development in n-amyl acetate solvent at room temperature for 60 seconds. Conformal TiO_2 layer with a thickness of approximately 70 nm was deposited by an atomic layer deposition system (Picosun) using titanium tetrachloride and H_2O as precursors at a reactor temperature of 130 °C. Subsequently, CHF_3 plasma in an inductively coupled plasma-reactive ion etching (ICP-RIE, Oxford system 100) was performed to blank- etch the TiO_2 layer until the ZEP 520A resist was exposed. Here the etching conditions were 20 sccm of CHF_3 at 50 W bias power/500 W induction power at an operating pressure of 10 mTorr, which resulted in a TiO_2 etching rate of ~20 nm per minute. Finally, O_2 plasma with small addition of CHF_3 was used to fully remove the remaining ZEP resist.

Measurement procedure. The laser beam collimated by a fiber collimator from a supercontinuous laser (NKT SuperKEXR-20) passed through a polarizer and a quarter-wave plate to obtain a left-handed circularly polarized light. Then, a 4*f*-system (L1 and L2 with focal lengths of 30 mm and 100 mm) was used to obtain an expanded collimated laser beam. To match the beam width with the size of each region of the metasurface, another lens L3 (focal length of 150mm) was used to focus the beam to a spot size of 30 μm. The focused beam was incident onto the statistical metasurface, and the movement of the statistical metasurface along the *x*-direction was controlled by an electric translation stage (e-X). Before measurement, the statistical metasurface and translation stage (e-X) need to be calibrated by a three-dimensional translation stage and a rotating stage. The coherence of the beam has been changed when passing through the statistical metasurface, and the instantaneous intensity of the transmitted light was captured by an imaging system, which contains an objective (Obj1), a tube lens (TL), and a CCD camera. Another quarter-wave plate and polarizer pair were employed to filter the right-handed circularly polarized component of the signals. In the experiments, we measured the light distributions at a plane with a distance of 120 μm away from the metasurface. The convergence of the measured coherence can be found in Supplementary Figs. 4 and 5.

Data availability. The data that support the finding of this study are available from the corresponding author upon request.

References

1 Zernike & Frederik. The concept of degree of coherence and its application to optical problems. *Physica* **5**, 785-795 (1938).

2 Goodman, J. W. *Statistical Optics*. (John Wiley & Sons, 2015).

3 Kato, Y. *et al.* Random phasing of high-power lasers for uniform target acceleration and plasma-instability suppression. *Phys. Rev. Lett.* **53**, 1057-1060 (1984).

4 Vidal, I., Fonseca, E. J. S. & Hickmann, J. M. Light polarization control during free-space propagation using coherence. *Phy. Rev. A* **84** (2011).

5 Bina, M. *et al.* Backscattering differential ghost imaging in turbid media. *Phys. Rev. Lett.* **110**, 083901 (2013).

6 Scarcelli, G., Berardi, V. & Shih, Y. Can two-photon correlation of chaotic light be considered as correlation of intensity fluctuations? *Phys. Rev. Lett.* **96**, 063602 (2006).

7 Ferri, F. *et al.* High-resolution ghost image and ghost diffraction experiments with thermal light. *Phys. Rev. Lett.* **94**, 183602 (2005).

8 Dogariu, A. & Amarande, S. Propagation of partially coherent beams: turbulence-induced degradation. *Opt. Lett.* **28**, 10-12 (2003).

9 Piquero, G. *et al.* Synthesis of partially polarized Gaussian Schell-model sources. *Opt. Commun.* **208**, 9-16 (2002).

10 Hyde, M. W., Bose-Pillai, S., Voelz, D. G. & Xiao, X. Generation of Vector Partially Coherent Optical Sources Using Phase-Only Spatial Light Modulators. Phys. Rev. Appl. 6 (2016).

11 Khorasaninejad, M. *et al.* Polarization-insensitive metalenses at visible wavelengths. *Nano Lett.* **16**, 7229-7234 (2016).

12 Liu, W. *et al.* Metasurface enabled wide-angle Fourier Lens. *Adv. Mater.* **30**, e1706368 (2018).

13 Manjappa, M. *et al.* Reconfigurable MEMS Fano metasurfaces with multiple-input-output states for logic operations at terahertz frequencies. *Nat. Commun.*

9, 4056 (2018).

14 Limonov, M. F., Rybin, M. V., Poddubny, A. N. & Kivshar, Y. S. Fano resonances in photonics. *Nat. Photonics* **11**, 543-554 (2017).

15 Koshelev, K. *et al.* Subwavelength dielectric resonators for nonlinear nanophotonics. *Science* **367**, 288-292 (2020).

16 Rybin, M. V. *et al.* High-Q supercavity modes in subwavelength dielectric resonators. *Phys. Rev. Lett.* **119**, 243901 (2017).

17 Yoda, T. & Notomi, M. Generation and annihilation of topologically protected bound states in the continuum and circularly polarized states by symmetry breaking. *Phys. Rev. Lett.* **125**, 053902 (2020).

18 Yu, N. *et al.* Light propagation with phase discontinuities: generalized laws of reflection and refraction. *Science* **334**, 333-337 (2011).

19 Maguid, E. *et al.* Photonic spin-controlled multifunctional shared-aperture antenna array. *Science* **352**, 1202-1206 (2016).

20 Pfeiffer, C. & Grbic, A. Metamaterial Huygens' surfaces: tailoring wave fronts with reflectionless sheets. *Phys. Rev. Lett.* **110**, 197401 (2013).

21 Picardi, M. F., Zayats, A. V. & Rodríguez-Fortuño, F. J. Janus and Huygens dipoles: near-field directionality beyond spin-momentum locking. *Phys. Rev. Lett.* **120**, 117402 (2018).

22 Kruk, S. *et al.* Invited Article: Broadband highly efficient dielectric metadevices for polarization control. *APL Photonics* **1**, 030801 (2016).

23 Yang, Y. *et al.* Dielectric meta-reflectarray for broadband linear polarization conversion and optical vortex generation. *Nano Lett.* **14**, 1394-1399 (2014).

24 Arbabi, A., Horie, Y., Bagheri, M. & Faraon, A. Dielectric metasurfaces for complete control of phase and polarization with subwavelength spatial resolution and high transmission. *Nature nanotechnology* **10**, 937-943 (2015).

25 Balthasar Mueller, J. P., Rubin, N. A., Devlin, R. C., Groever, B. & Capasso, F. Metasurface polarization optics: independent phase control of arbitrary orthogonal states of polarization. *Phys. Rev. Lett.* **118**, 113901 (2017).

26 Devlin, R. C., Ambrosio, A., Rubin, N. A., Mueller, J. B. & Capasso, F.

Arbitrary spin-to–orbital angular momentum conversion of light. *Science* **358**, 896-901 (2017).

27 Chen, S., Li, Z., Liu, W., Cheng, H. & Tian, J. From single-dimensional to multidimensional manipulation of optical waves with metasurfaces. *Adv. Mater.* **31**, e1802458 (2019).

28 Xu, H. X. *et al.* Chirality-assisted high-efficiency metasurfaces with independent control of phase, amplitude, and polarization. *Adv. Opt. Mater.* (2018).

29 Zuo, R., Liu, W., Cheng, H., Chen, S. & Tian, J. Breaking the Diffraction Limit with Radially Polarized Light Based on Dielectric Metalenses. *Adv. Opt. Mater.* **6** (2018).

30 Jang, M. *et al.* Wavefront shaping with disorder-engineered metasurfaces. *Nat. Photonics* **12**, 84-90 (2018).

31 Wolf, E. *Introduction to the Theory of Coherence and Polarization of Light*. (Cambridge University Press, 2007).

32 Liang, C. *et al.* Overcoming the classical Rayleigh diffraction limit by controlling two-point correlations of partially coherent light sources. *Opt. Express* **25** (2017).

33 Zhao, C. & Cai, Y. Trapping two types of particles using a focused partially coherent elegant Laguerre–Gaussian beam. *Opt. Lett.* **36**, 2251-2253 (2011).

34 Overvig, A. C. *et al.* Dielectric metasurfaces for complete and independent control of the optical amplitude and phase. *Light: Sci. Appl.* **8**, 92 (2019).

35 Eichmann, U. *et al.* Young's interference experiment with light scattered from two atoms. *Phys. Rev. Lett.* **70**, 2359 (1993).

36 McEliece, R. & Mac Eliece, R. J. *The Theory of Information and Coding*. Vol. 86 (Cambridge University Press, 2002).

37 Khorasaninejad, M. & Capasso, F. Metalenses: Versatile multifunctional photonic components. *Science* **358** (2017).

38 Liu, W. *et al.* Aberration-corrected three-dimensional positioning with a single-shot metalens array. *Optica* **7** (2020).

39 Magatti, D., Gatti, A. & Ferri, F. Three-dimensional coherence of light speckles:

Experiment. *Phys. Rev. A* **79** (2009).

40 Wang, F. & Cai, Y. Experimental observation of fractional Fourier transform for a partially coherent optical beam with Gaussian statistics. *J. Opt. Soc. Am. A* **24**, 1937-1944 (2007).

41 Friberg, A. T. & Sudol, R. J. J. O. C. Propagation parameters of Gaussian Schell-model beams. *Opt. Commun.* **41**, 383-387 (1982).

42 Arbabi, E. *et al.* MEMS-tunable dielectric metasurface lens. *Nat. Commun.* **9**, 812 (2018).

43 Forbes *et al.* Structured light. *Nat. Photonics* **15**, 253-262 (2021).

Acknowledgements

This work was supported by the National Key Research and Development Program of China (2016YFA0301102, 2017YFA0303800, and 2019YFA0705000), the National Natural Science Fund for Distinguished Young Scholar (11925403), the National Natural Science Foundation of China (11974193, 11974218, 11904183, 11904181, 91856101, and 11774186), Natural Science Foundation of Tianjin for Distinguished Young Scientists (18JCJQJC45700), the China Postdoctoral Science Foundation (2018M640224), Innovation Group of Jinan (2018GXRC010), and Local Science and Technology Development Project of the Central Government (YDZX20203700001766); The metasurface nanofabrication was performed at the ACT node of the Australian National Fabrication Facility.

Author contributions

W.L., H.C., Y.C., and S.C. initiated the idea. L.L., W.L., F.W., and H.C. performed the theoretical analysis, numerical simulations and experiments. D.C. fabricated the

samples. L.L., W.L., H.C., J.T., Y.C., and S.C. prepared the manuscript. S.C. supervised the project. All the authors contributed to the analyses and discussions of the manuscript.

Additional information

Supplementary Information is available online at XXX or from the author.

Competing financial interests: The authors declare no competing financial interests.

Figures

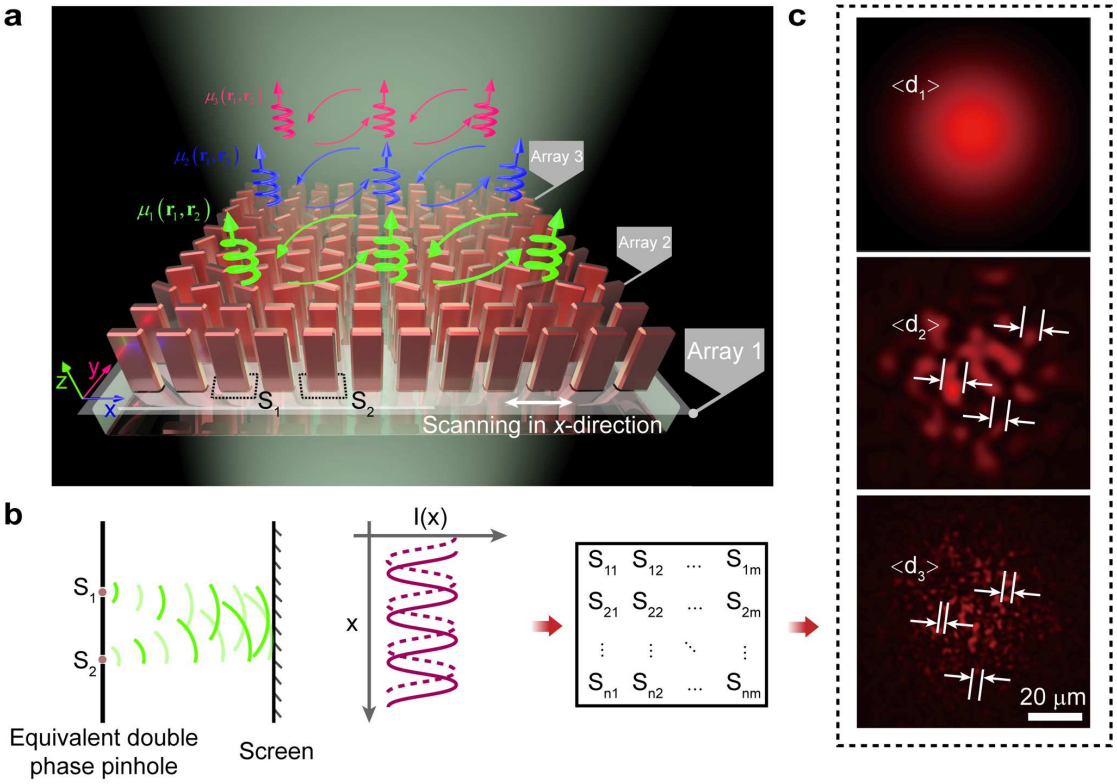

Fig. 1 | Design of the statistical metasurface and its operation principle. a, Schematic of the statistical metasurface that can generate light beams with different degrees of spatial coherence by mechanically controlling the statistical metasurface along the *x*-direction. **b**, Diagram of the coherence of a wave generated by any two points on the statistical metasurface. Different equivalent phase pinholes form phase arrays with different statistical properties. **c**, Theoretical intensity distributions of light speckles generated by different arrays on the statistical metasurface. The smaller the size <d> of the speckle is, the lower the spatial coherence of the transmitted beam will be.

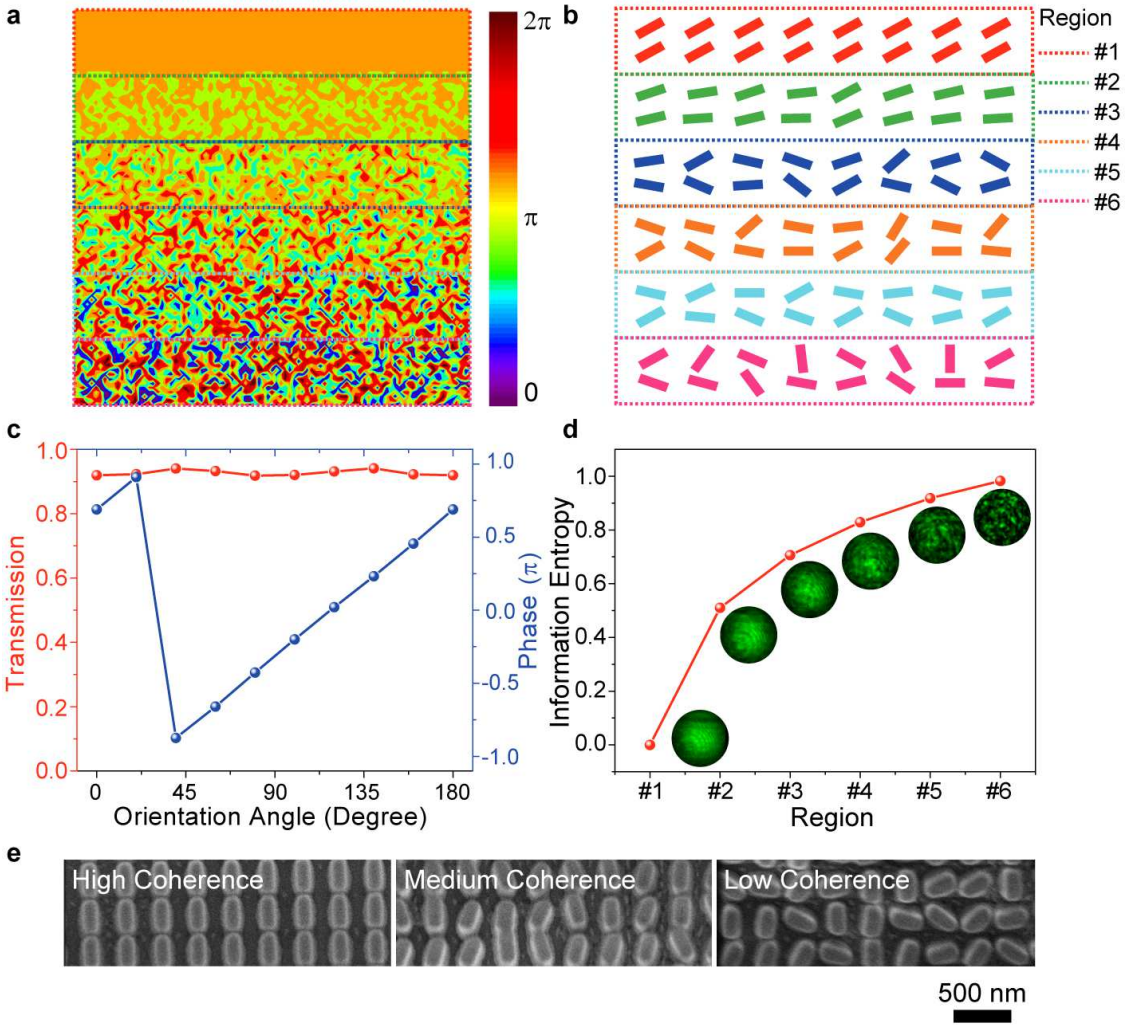

Fig. 2 | Design and fabrication of the dielectric nanofins array. a, The phase distribution of the designed statistical metasurface with 6 different pre-defined spatial coherence in different rows. **b**, Schematic of the arrangement of the nanofins arrays corresponding to different arrays in **a**. **c**, Simulated cross-polarization transmission and phase abrupt as a function of different orientation angles of the nanofins at the operating wavelength of 532 nm. **d**, Calculated information entropy of the phased arrays and the instantaneous intensity of the transmitted light in each region. **e**, Scanning electron microscopy (SEM) images of the fabricated metasurfaces for three different DOC.

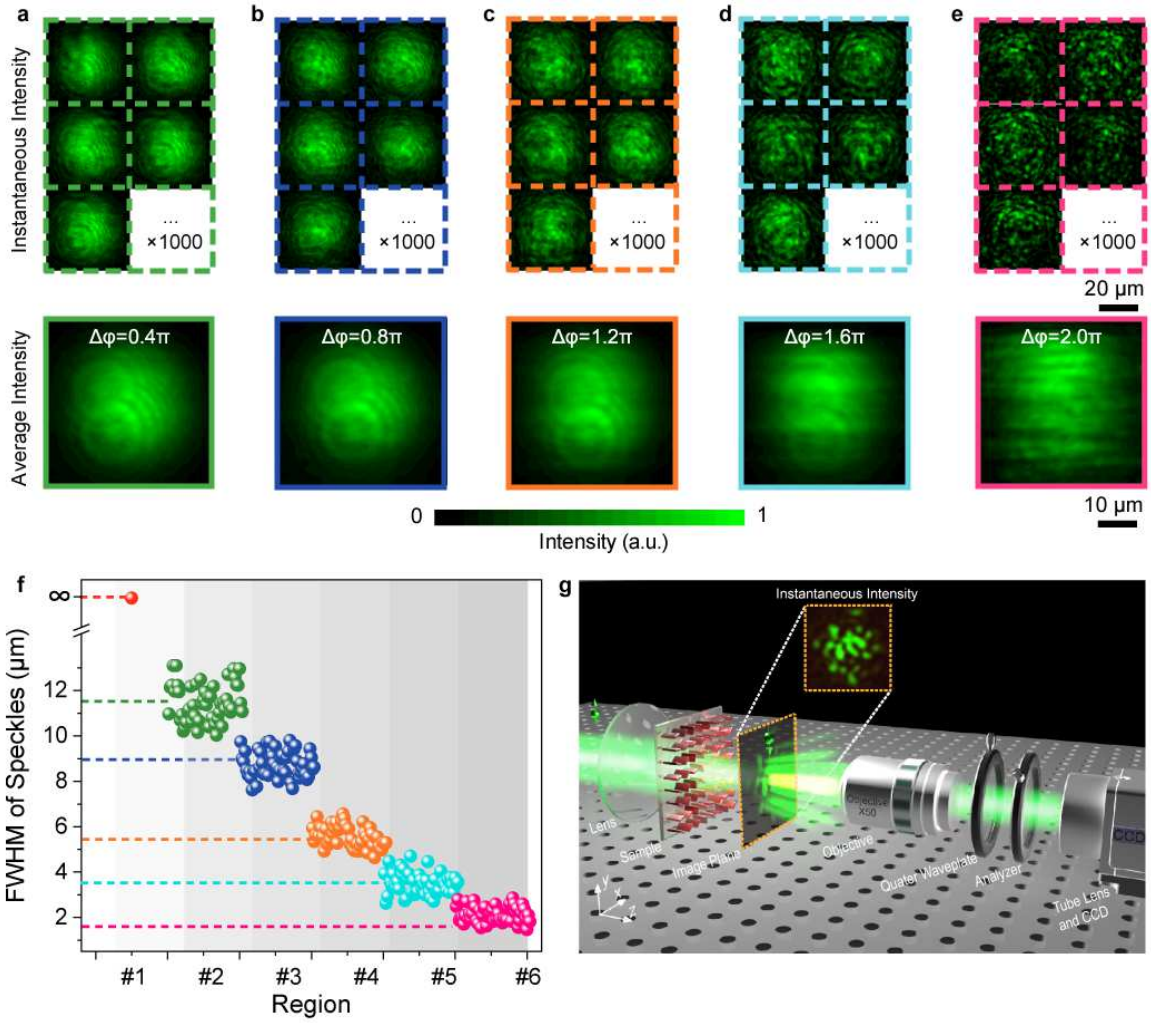

Fig. 3 | Measurement of the transmitted statistical speckles. a-e, Experimental instantaneous intensity distributions (top) and corresponding average intensity of ×1000 instantaneous intensity (bottom) for different PFRs. **f**, Fluctuation of the measured FWHM of the speckles induced by the disordered arrangement of the nanofins. **g**, Experimental setup to capture the instantaneous intensity distributions of the Gaussian-envelope beams. The statistical metasurface sample locates at $z = 0$ in the laboratory coordinate.

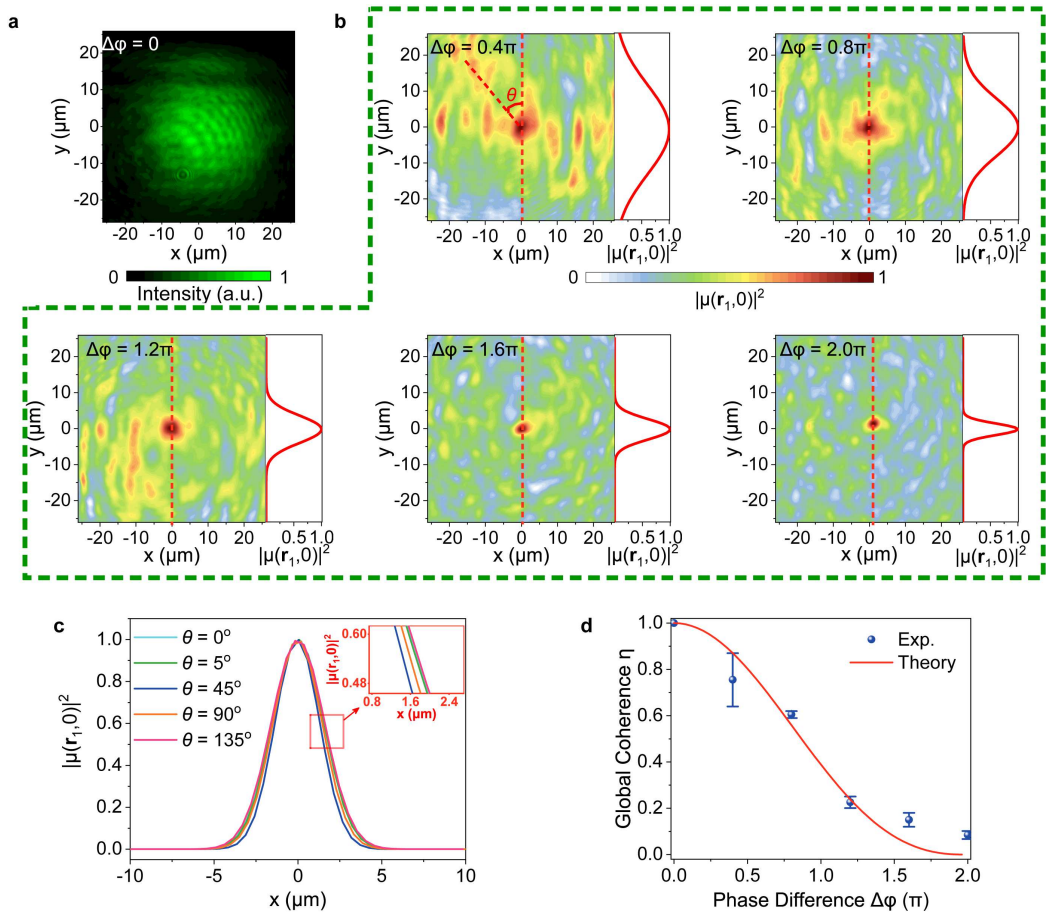

Fig. 4 | Spatial coherence manipulation based on the statistical metasurfaces. a, Intensity profile of the fully coherent Gaussian beam at the z = 120 μm cut-plane. **b**, Experimental distributions of the square of the modulus of the DOC for different PFRs and the Gaussian curve-fitting along the x = 0 cut-lines. The FWHMs of the Gaussian curves indicate the coherent length of the generated partially coherent beams. **c**, Gaussian curve-fitting of $|\mu(\mathbf{r}_1, 0)|^2$ for $\Delta\varphi = 2\pi$ for different cut-line orientation angles θ, which is defined as the intersection with the $+y$ direction shown in **a**. Inset: zoom in the influence of θ. **d**, Comparison between the calculated global DOC based on measurements and the theoretical results respectively. The error bar indicates the statistical fluctuation induced by the incomplete sets of cut-lines and measurements.

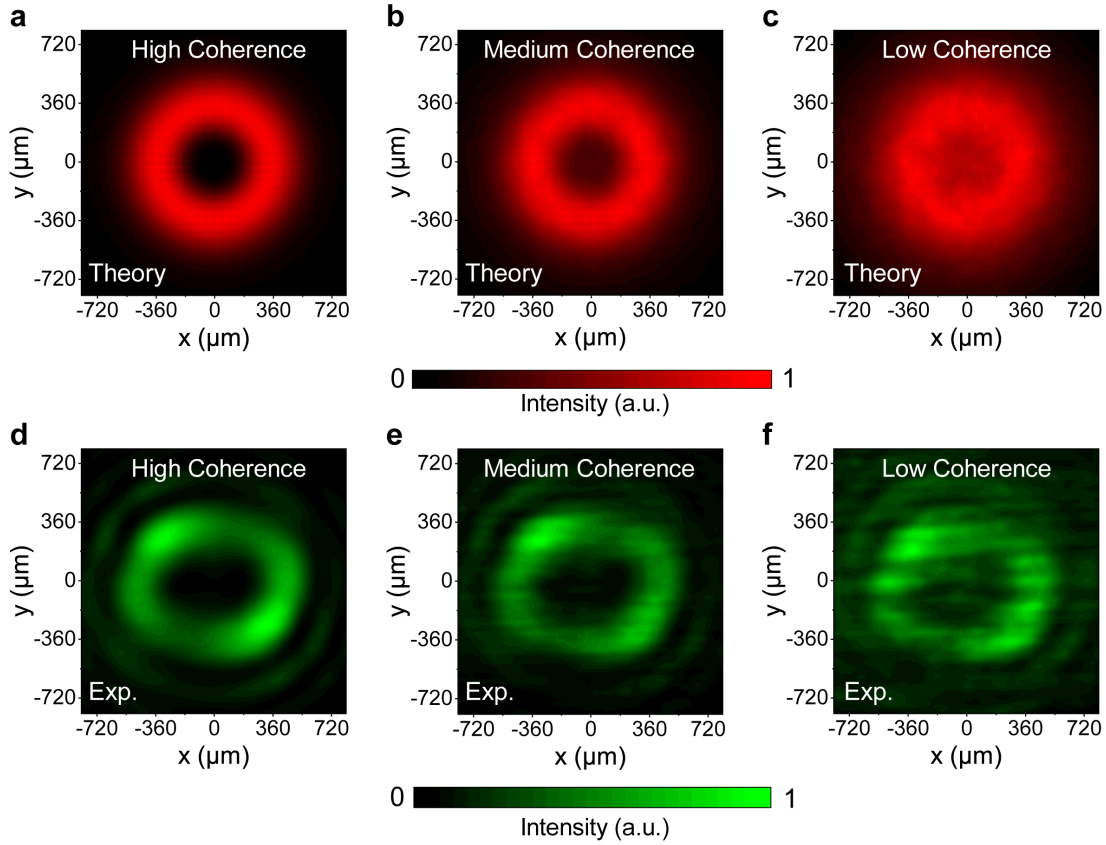

Fig. 5 | Spatial coherence manipulation of the vortex beams. a-c, Theoretical calculations of the intensity distributions of partially coherent vortex beams with different coherences. **d-f**, Corresponding measured intensity distributions of the partially coherent vortex beams with different coherences. The central dark spot of the doughnut intensity profile for the partially coherent vortex beam becomes weaker for lower coherence due to the disordered phase distribution.

Supplementary Files

This is a list of supplementary files associated with this preprint. Click to download.

- SupplementaryInformation.doc
- Supplementaryvideo1.mp4